Hybridization of Subgap States in One-Dimensional Superconductor-Semiconductor Coulomb Islands

E. C. T. O'Farrell,[1] A. C. C. Drachmann,[1] M. Hell,[1,2] A. Fornieri,[1] A. M. Whiticar,[1] E. B. Hansen,[1] S. Gronin,[3,4] G. C. Gardner,[3,4] C. Thomas,[3,4] M. J. Manfra,[3,5,6,4] K. Flensberg,[1] C. M. Marcus,[1] and F. Nichele[1]

[1]*Center for Quantum Devices and Station Q Copenhagen, Niels Bohr Institute, University of Copenhagen, Universitetsparken 5, 2100 Copenhagen, Denmark*

[2]*Division of Solid State Physics and NanoLund, Lund University, Box 118, S-22100 Lund, Sweden*

[3]*Department of Physics and Astronomy and Station Q Purdue, Purdue University, West Lafayette, Indiana 47907, USA*

[4]*Birck Nanotechnology Center, Purdue University, West Lafayette, Indiana 47907, USA*

[5]*School of Materials Engineering, Purdue University, West Lafayette, Indiana 47907, USA*

[6]*School of Electrical and Computer Engineering, Purdue University, West Lafayette, Indiana 47907, USA*

(Received 25 April 2018; published 19 December 2018)

We present measurements of one-dimensional superconductor-semiconductor Coulomb islands, fabricated by gate confinement of a two-dimensional InAs heterostructure with an epitaxial Al layer. When tuned via electrostatic side gates to regimes without subgap states, Coulomb blockade reveals Cooper-pair mediated transport. When subgap states are present, Coulomb peak positions and heights oscillate in a correlated way with magnetic field and gate voltage, as predicted theoretically, with (anti) crossings in (parallel) transverse magnetic field indicating Rashba-type spin-orbit coupling. Overall results are consistent with a picture of overlapping Majorana zero modes in finite wires.

DOI: 10.1103/PhysRevLett.121.256803

The prediction that a topological superconductor is realized by combining accessible and well-understood materials [1,2] prompted an intense experimental effort into superconductor-semiconductor hybrids. Open geometries, i.e., without charging energy, have been instrumental to demonstrate transport behavior consistent with Majorana zero modes (MZMs) [3–6]. However, finite charging energy is essential in schemes to probe non-Abelian exchange statistics of MZMs and implement topological quantum information processing [7–11]. In a superconducting Coulomb island, the Coulomb blockade (CB) period is a probe of the lowest subgap state energy [12,13], making it a viable tool to study MZMs. This geometry was investigated by Albrecht *et al.* [14], who showed that, in short wires, modes are no longer fixed at zero energy as the magnetic field increases, but instead oscillate. Oscillations in the CB period might, however, also occur at level crossings of states having no topological character. Numerical simulations suggested several such situations [15]: multiple subband occupancy, the presence of trivial Andreev bound states, or, simply, if the spin-orbit interaction (SOI) is negligible.

Here, we experimentally investigate two aspects of one-dimensional superconductor-semiconductor wires relevant to the topological phase transition: the hybridization of particlelike and holelike subgap states and the spin structure of those hybridized states. The wire-shaped Coulomb islands are lithographically patterned using a two-dimensional electron gas (2DEG) of InAs with an epitaxial layer of Al [16]. Previous work has shown discrete zero-energy modes can be induced in this heterostructure [5,17]. We first show that the system can be tuned to a two-electron ($2e$) periodic CB, indicative of no subgap states below the charging energy E_C and the absence of quasiparticle poisoning. When discrete subgap states are present CB peaks spacing oscillates both with gate voltage, and magnetic fields applied in the plane of the 2DEG. We focus on in-plane fields applied parallel ($B_\parallel$) or transverse ($B_\perp$) to the wire to elucidate the SOI structure. Coulomb peak spacing oscillations correlate with oscillations in peak conductance, as predicted for extended subgap states in clean Majorana wires undergoing a crossover in the spectral weight of their electronlike and holelike components [18]. Investigating CB spacing as a function of field orientation, we conclude subgap states are subject to a dominant Rashba-type SOI, and we provide a lower bound for the Rashba parameter.

Figure 1(a) shows a schematic of the device, the measurement setup, and the field orientations used in this work. Following the approach of Ref. [17], an Al wire, with dimensions L and W, is etched into the epitaxial Al layer (blue) on top of the III-V heterostructure (gray), with the InAs quantum well 10 nm below the surface; images of several devices are shown in Ref. [19]. Contact to the island is made via extended planes of the original Al epilayer. Ti/Au gates (yellow) are deposited on an atomic layer deposition grown HfO_2 dielectric. The voltage V_W depletes the 2DEG surrounding the Al stripe, but not below it, and

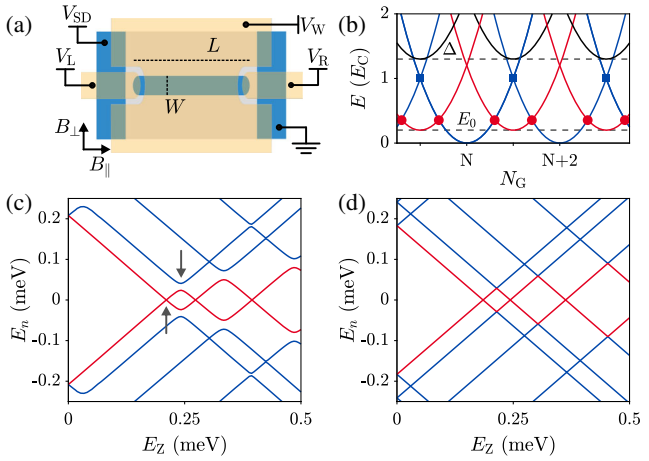

FIG. 1. (a) Device schematic, together with gating and magnetic field orientation definitions. Al is represented in blue, the III-V heterostructure in gray, and the gates in yellow, voltages V_L, V_R, and V_W are applied to the gates and V_{SD} is applied to one Ohmic contact. (b) The energy spectrum, in units of E_C, of the superconducting quantum dot versus the gate-induced occupancy N_G. N (blue) represents an even charge state; at odd occupancies a discrete subgap state with energy E_0, in this case $E_0 < E_C$, is shown (red) as well as the quasiparticle continuum at $E > \Delta$ (black). (c) Calculated energy spectrum of subgap states versus the Zeeman energy for magnetic field orthogonal to SOI magnetic field, the lowest pair of subgap states is shown in red. The left arrow indicates crossing of states with opposite parity, the right arrow indicates anticrossing of states with the same parity. (d) The energy spectrum against the Zeeman energy for magnetic field parallel to SOI magnetic field, the lowest pair of subgap states is shown in red.

tunes the chemical potential of the resulting Coulomb island. Voltages V_R and V_L tune the transmission of the right and left tunneling barrier, respectively. We present results from two nominally identical devices (device 1 and 2) with $L = 750$ nm and $W = 80$ nm parallel to the $[0\bar{1}\,\bar{1}]$ and $[01\bar{1}]$ crystal directions, respectively. Data on an additional $L = 750$ nm sample that did not show discrete subgap states, and did not demonstrate the correlation between CB spacing and conductance that is reported here, are shown in Ref. [19], together with data from two longer islands that showed a decreased magnitude of subgap state oscillations consistent with Ref. [14]. Transport measurements were performed in a dilution refrigerator with a base temperature of 20 mK via conventional lock-in techniques. A voltage bias V_{SD} was applied to one Ohmic contact while the current and four-terminal voltage were recorded and used to calculate the differential conductance G. Devices 1 and 2 were aligned parallel and perpendicular, respectively, to the major axis of a vector magnet.

For a superconducting Coulomb island, with negligible level spacing, tunnel coupled to metallic leads, the lowest energy state with N charges is given by $E(N, N_G) = E_C(N_G - N)^2 + E_0(N \mod 2)$, where N_G is the gate-induced occupancy, E_0 is the energy of the lowest unpaired quasiparticle state, i.e., equal to the gap Δ in the absence of subgap states, and E_C is the charging energy [see Fig. 1(b)]. At zero bias, charge flows at degeneracy $E(N, N_G) = E(N + \delta, N_G)$; these are CB peaks. For $E_0 > E_C$, transport occurs at blue squares in Fig. 1(b); the lowest energy state always has even occupation [12,23]. However, when $E_0 \leq E_C$, transport occurs in the odd state too [red dots in Fig. 1(b)], making CB spacing a probe for E_0.

The combined effect of SOI and Zeeman field drives discrete states into the superconducting gap, leading to a topological phase transition and modes with $E_0 \to 0$ for one-dimensional islands [1,2]. The calculated energy spectrum for a finite-length wire, versus Zeeman energy E_Z, is shown in Figs. 1(c) and 1(d) for magnetic field applied perpendicular and parallel to the direction of the wire, respectively. The model, described in Refs. [19,24], assumes a Rashba-like SOI, $H_{SOI} = \alpha(\sigma_x p_y - \sigma_y p_x)\tau_z$, where α is the Rashba parameter, τ_i and σ_i are Pauli matrices for particle-hole and spin space, respectively, p is the momentum, and the y axis is defined to be parallel to the wire. That is, the SOI magnetic field lies in the plane of the 2DEG and perpendicular to the wire. As for conventional semiconductor nanostructures, SOI mixes spin states [25–27], leading to the anticrossing of isoparity subgap states following the first zero-energy crossing of modes with opposite parity [up-pointing and down-pointing arrows in Fig. 1(c), respectively]. In contrast, when the external magnetic field is aligned to the SOI magnetic field, spin-up and spin-down levels cross.

To investigate these spectral features experimentally, we tuned the subgap spectrum of the wire by adjusting the voltage V_W, which modifies both the chemical potential and the spatial confinement of electrons below the Al. The lowest subgap state energy was then probed by measuring the CB spacing while varying V_L to change the island occupancy keeping the spectrum unaltered [19]. Figures 2(a)–2(c) show Coulomb diamonds versus V_L at $B_\parallel = 0$, 2, and 4 T and for $V_W = -694$ mV. At $B = 0$, enhanced conductance at $V_{SD} = 0$, together with regular features at $V_{SD} \approx 2\Delta/n$, where n is an integer, are attributed to a supercurrent and multiple Andreev reflection with the superconducting leads, respectively [19]. At 2 T these features were absent and the spectrum was similar to that reported for superconducting devices with metallic leads [28], consistent with the extended Al planes having a finite and smooth subgap density of states at $B \gtrsim 0.1$ T, which is suitable for spectroscopy [17]. At 4 T the system was normal and $E_C = 125$ μeV.

Figure 2(d) shows zero-bias conductance versus $B_\parallel$ and V_L. The spacing averaged over even (odd) valleys $\langle s_{e(o)} \rangle$ [Fig. 2(e)] was constant up to 2.25 T, indicating no subgap states, before decreasing linearly to half the zero-field value, when the normal state is reached. We refer to CB periodicities as $2e$, even or odd (e or o) and $1e$, respectively. Also shown is the normalized conductance ratio $\langle \gamma \rangle = \langle (g_e - g_o)/(g_e + g_o) \rangle$ averaged over pairs of peaks.

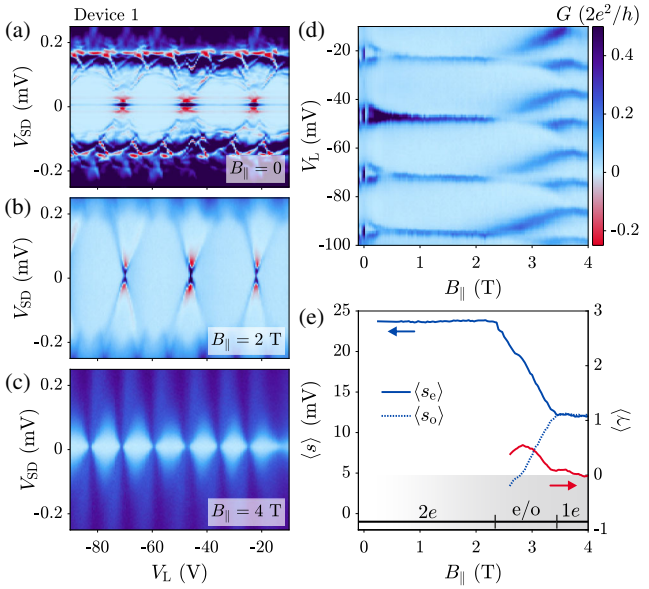

FIG. 2. (a)–(c) Bias spectroscopy of device 1 at $V_W = -694$ mV and $B_\parallel = 0, 2, 4$ T. (d) Conductance at zero bias as a function of V_L and $B_\parallel$. (e) Left-hand axis: $\langle s_{e(o)} \rangle$ spacing of valleys with even (solid) and odd (dotted) parity averaged over valleys for data in (d); right-hand axis: conductance ratio $\langle \gamma \rangle = \langle (g_e - g_o)/(g_e + g_o) \rangle$ averaged over pairs of peaks. For data in (d), gray region denotes $\langle \gamma \rangle \leq 0$.

This quantity was found to become zero in the normal state; its significance is discussed below in detail. Temperature dependence yielded $\Delta = 260$ μeV at $B_\parallel = 0.25$ T, and we estimated a parity lifetime ≥ 1 ms [19].

We next investigate the situation where discrete subgap states were present. Figure 3(a) shows the zero-bias conductance versus V_W and V_L at $B_\parallel = 2$ T. As V_W was swept from the regime of Fig. 2, to more negative values, $2e$ periodic CB peaks were split, their spacing became even or odd and oscillated about a $1e$ periodicity, with a further reduction of V_W, $2e$ charging was reestablished. We interpret this behavior as a discrete subgap state entering the spectrum; we further justify this interpretation in Ref. [19]. The average peak spacings $\langle s_{e(o)} \rangle$ versus V_W are shown in Fig. 3(b) (left-hand axis), together with the average peak amplitude $\langle \gamma \rangle$. Similar measurements as a function of V_R gave compatible results [19], with CB period almost independent of extended ranges of V_L and V_R, that indicated a state not localized to the ends of the wire. We also note that oscillations in $\langle \gamma \rangle$ were correlated with oscillations in $\langle s_{e(o)} \rangle$: zero crossings of $\langle \gamma \rangle$ matched extrema in $\langle s_{e(o)} \rangle$. Figures 3(c) and 3(e) show the evolution in $B_\parallel$ at $V_W = -704$ mV. E_0 crossed zero energy at $B_\parallel = 0.75$ T, and then oscillated with a maximum at $B_\parallel = 1.8$ T. Figures 3(d) and 3(f) show the conductance ratio and peak spacing for a comparable regime in device 2 under $B_\perp$. In Fig. 3(f), zero crossings of $\langle \gamma \rangle$ are also correlated with extrema in spacing as expected; however, the correlation depends sensitively and nonuniquely on the

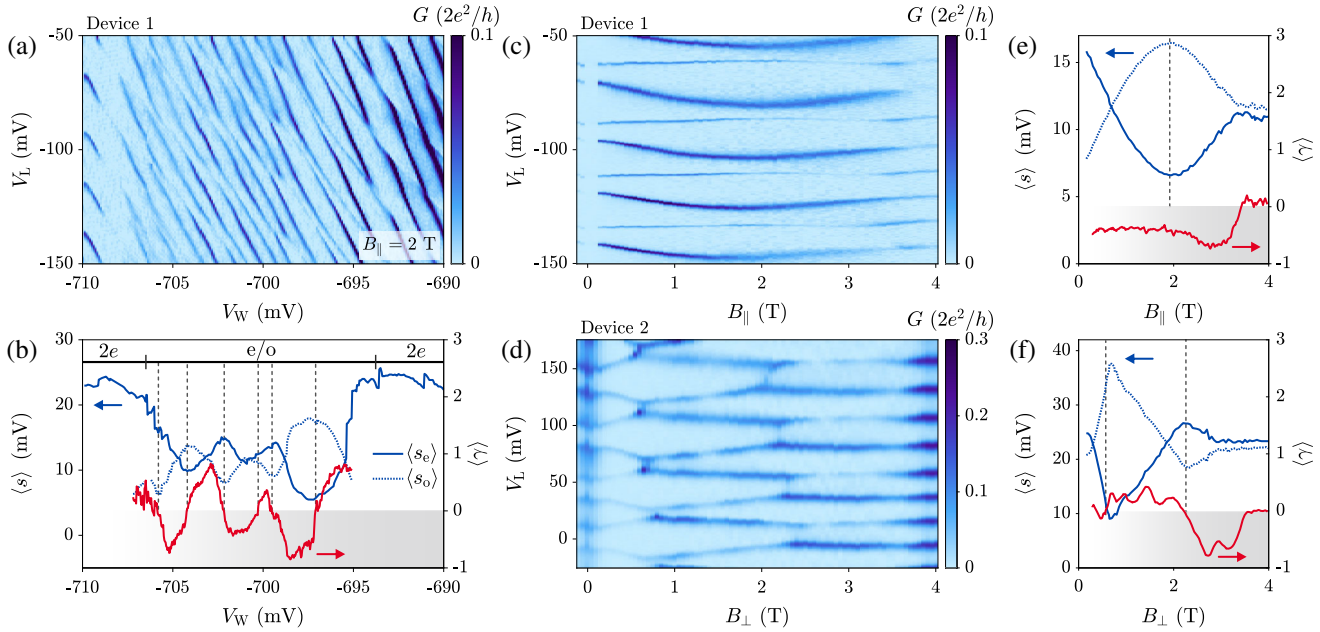

FIG. 3. (a) Zero-bias conductance as a function of V_L and V_W for device 1 at $B_\parallel = 2$ T. (b) Left-hand axis: magnitude of the CB peak spacing of (a) averaged over peaks (in units of V_L). Right-hand axis: $\langle \gamma \rangle = \langle (g_e - g_o)/(g_e + g_o) \rangle$, dashed lines correspond to zero crossings of $\langle \gamma \rangle$. (c) Zero-bias conductance as a function of V_L and $B_\parallel$ at $V_W = -704$ mV for device 1. (d) Zero-bias conductance as a function of V_L and $B_\perp$ for device 2; for gating configuration see Ref. [19]. (e) Analysis as in (b), for data in (c). Here the dashed line indicates a maximum in $\langle s_{e(o)} \rangle$. (f) Analysis as in (b), for data in (d).

Andreev bound state description and therefore we do not model this relationship. The correlation becomes less evident in Fig. 3(e), presumably due to the small number of oscillations as a function of $B_\parallel$. In the Supplemental Material [19] we provide additional data on device 2 and compare the oscillations in $\langle s_{e(o)} \rangle$ with direct tunneling spectroscopy of subgap states. The effective g factor of these states is < 5, consistent with a small orbital magnetic field effect [29].

The observed relationship between $s_{e(o)}$ and γ was predicted to be characteristic of oscillating subgap states in uniform nanowires [18,19]. For a hybridized Majorana mode, oscillations in gate potential and magnetic field reflect oscillations in the electron-hole and spin components of the wave function, and vanish in the limit $L \to \infty$. The state of Fig. 3(a) is compatible with such an interpretation. Similarly, the oscillations seen in Fig. 3(d) for $B_\perp$ are consistent with a change in the lowest energy state, which dominates transport through the wire. Such a state is also expected to give rise to a Majorana mode for $B_\parallel$. Correlation between CB peaks spacing and amplitude, with a $\pi/2$ phase shift in their oscillations, was not previously reported and provides an additional tool for the identification of MZMs in Coulomb islands. In contrast, localized Andreev states [30] are expected to show no particular relation between γ and $s_{e(o)}$ [18].

Oscillations of $\langle s_{e(o)} \rangle$ in $B_\parallel$ or $B_\perp$ were qualitatively different: the smooth curvature in Fig. 3(d) contrasts with the sharp kinks in Fig. 3(f). This behavior reflects a different spin hybridization of subgap states for $B_\parallel$ and $B_\perp$. Figure 4(a) shows bias spectroscopy at several $B_\parallel$ in the vicinity of the spacing maximum in Fig. 3(c). Negative differential conductance indicated blocking of quasiparticle tunneling into the state [23]. This enabled us to estimate a quasiparticle tunneling rate, which, following the method of Ref. [28], provides an estimate of the parity lifetime of this state, ≥ 100 μs at $B_\parallel = 2$ T [19]. As $B_\parallel$ increased, the excited state moved to lower energy; however, it did not reach the lowest energy state. Similarly, bias spectroscopy in $B_\perp$ for device 2 [Fig. 4(b)] showed a discrete energy level was present in the vicinity of the first oscillation in Fig. 3(e). This showed the level became degenerate with the ground state energy at $B_\parallel = 1$ T. The magnitude of negative differential conductance was strongly reduced for $B_\perp$, which indicated a weakened blocking effect. Enhanced conduction within the valleys in Fig. 3(d), around maxima in the spacing, may be a signature of the orbital Kondo effect at small energy scales around degeneracy [31], but is not visible for $B_\parallel$.

To measure crossing and anticrossing precisely, we fixed a finite V_{SD} and varied B. Figures 4(c) and 4(d) show the results for $B_\parallel$ and $B_\perp$ at $V_{SD} = 150$ and 75 μV, respectively; for cross sections, see Ref. [19]. For $B_\parallel$, the lowest energy state anticrossed with an excited state and then moved back towards zero energy. The energy splitting averaged over the peaks of Fig. 3(c) was ~ 60 μeV,

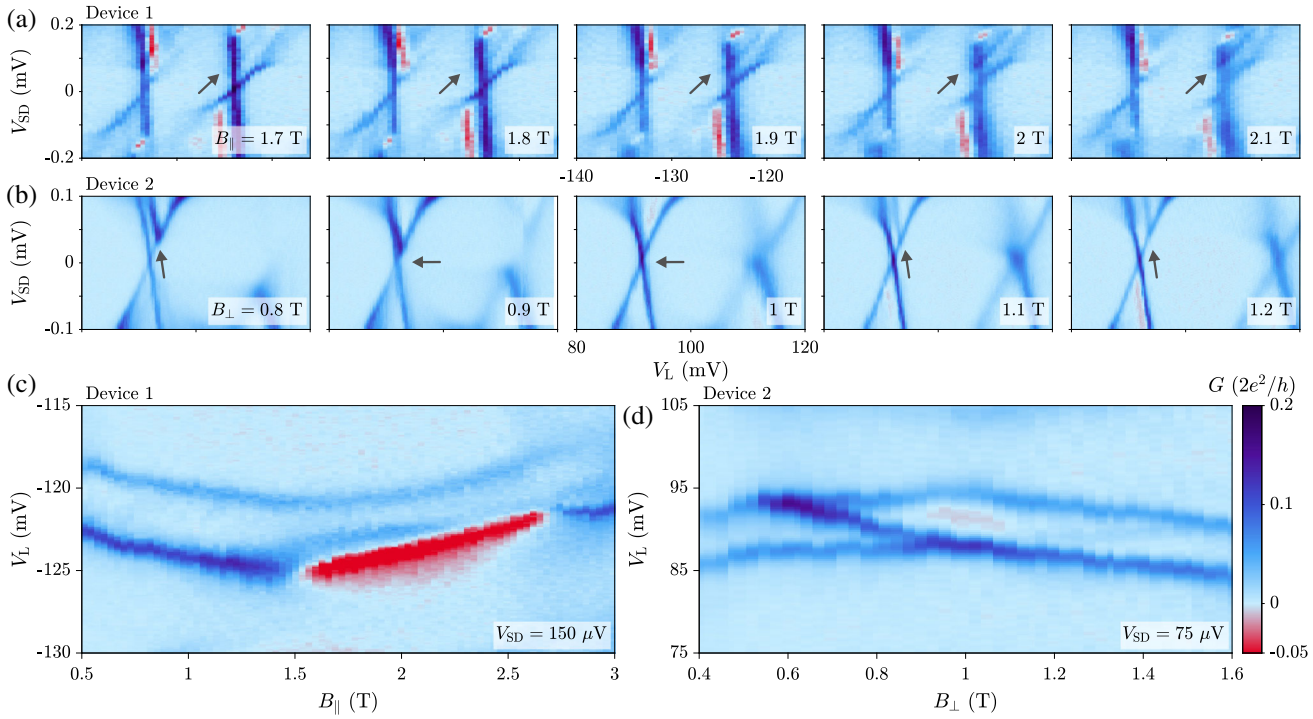

FIG. 4. (a) Bias spectroscopy at various $B_\parallel$ around the maximum in peak spacing in Fig. 3(c). Arrows show the position of an excited state, red color scale corresponds to negative differential conductance. (b) Similar results as in (a) for device 2 in $B_\perp$ for fields around $B_\perp = 1$ T. (c) G at $V_{SD} = 150$ μV in $B_\parallel$ showing anticrossing of lowest and first excited subgap states. (d) G at $V_{SD} = 75$ μV in $B_\perp$ showing crossing of lowest and first excited subgap states.

corresponding to the minigap denoted by a down-pointing arrow in Fig. 1(c). Instead, for $B_\perp$, the lowest energy and excited state exchanged position. The observation that parity states anticross for $B_\parallel$ and cross for $B_\perp$ is an indication that the dominant SOI in this system is of Rashba type. Further analysis [19] used the experimentally obtained anticrossing energy [Fig. 4(c)] to estimate a lower bound of the Rashba parameter, $\alpha \geq 120$ meV Å. This bound is compatible with the value extracted from anti-localization measurements ($\alpha = 280$ meV Å) of a similar heterostructure with all the Al removed [16].

In conclusion, InAs-Al 2DEG based hybrids are a suitable platform to fabricate clean superconductor-semiconductor Coulomb islands, with long parity lifetimes of bound states. Oscillations in energy of subgap states as a function of in-plane magnetic field and gate voltage are consistent with oscillations of parity bands of a Majorana mode. In the light of our results, devices of this kind offer great promise for MZM physics in multi-island geometries.

This work was supported by Microsoft Corporation, the Danish National Research Foundation, and the Villum Foundation. We thank J. Folk, J. Gamble, M. Leijnse, C. Olsen, and H. Suominen for useful discussions.

[1] R. M. Lutchyn, J. D. Sau, and S. Das Sarma, Phys. Rev. Lett. **105**, 077001 (2010).
[2] Y. Oreg, G. Refael, and F. von Oppen, Phys. Rev. Lett. **105**, 177002 (2010).
[3] V. Mourik, K. Zuo, S. M. Frolov, S. Plissard, E. Bakkers, and L. P. Kouwenhoven, Science **336**, 1003 (2012).
[4] M. Deng, S. Vaitiekėnas, E. B. Hansen, J. Danon, M. Leijnse, K. Flensberg, J. Nygård, P. Krogstrup, and C. M. Marcus, Science **354**, 1557 (2016).
[5] F. Nichele, A. C. C. Drachmann, A. M. Whiticar, E. C. T. O'Farrell, H. J. Suominen, A. Fornieri, T. Wang, G. C. Gardner, C. Thomas, A. T. Hatke *et al.*, Phys. Rev. Lett. **119**, 136803 (2017).
[6] H. Zhang, C.-X. Liu, S. Gazibegovic, D. Xu, J. A. Logan, G. Wang, N. van Loo, J. D. Bommer, M. W. de Moor, D. Car *et al.*, Nature (London) **556**, 74 (2018).
[7] L. Fu, Phys. Rev. Lett. **104**, 056402 (2010).
[8] D. Aasen, M. Hell, R. V. Mishmash, A. Higginbotham, J. Danon, M. Leijnse, T. S. Jespersen, J. A. Folk, C. M. Marcus, K. Flensberg *et al.*, Phys. Rev. X **6**, 031016 (2016).
[9] T. Karzig, C. Knapp, R. M. Lutchyn, P. Bonderson, M. B. Hastings, C. Nayak, J. Alicea, K. Flensberg, S. Plugge, Y. Oreg *et al.*, Phys. Rev. B **95**, 235305 (2017).
[10] S. Plugge, A. Rasmussen, R. Egger, and K. Flensberg, New J. Phys. **19**, 012001 (2017).
[11] D. Litinski, M. S. Kesselring, J. Eisert, and F. von Oppen, Phys. Rev. X **7**, 031048 (2017).
[12] M. T. Tuominen, J. M. Hergenrother, T. S. Tighe, and M. Tinkham, Phys. Rev. Lett. **69**, 1997 (1992).
[13] P. Lafarge, P. Joyez, D. Esteve, C. Urbina, and M. H. Devoret, Phys. Rev. Lett. **70**, 994 (1993).
[14] S. M. Albrecht, A. Higginbotham, M. Madsen, F. Kuemmeth, T. S. Jespersen, J. Nygård, P. Krogstrup, and C. M. Marcus, Nature (London) **531**, 206 (2016).
[15] C.-K. Chiu, J. D. Sau, and S. Das Sarma, Phys. Rev. B **96**, 054504 (2017).
[16] J. Shabani, M. Kjaergaard, H. Suominen, Y. Kim, F. Nichele, K. Pakrouski, T. Stankevic, R. M. Lutchyn, P. Krogstrup, R. Feidenhans *et al.*, Phys. Rev. B **93**, 155402 (2016).
[17] H. J. Suominen, M. Kjaergaard, A. R. Hamilton, J. Shabani, C. J. Palmstrøm, C. M. Marcus, and F. Nichele, Phys. Rev. Lett. **119**, 176805 (2017).
[18] E. B. Hansen, J. Danon, and K. Flensberg, Phys. Rev. B **97**, 041411 (2018).
[19] See Supplemental Material at http://link.aps.org/supplemental/10.1103/PhysRevLett.121.256803 for material and methods, and additional measurements, which includes Refs. [20–22].
[20] M. Kjærgaard, H. J. Suominen, M. P. Nowak, A. R. Akhmerov, J. Shabani, C. J. Palmstrøm, F. Nichele, and C. M. Marcus, Phys. Rev. Applied **7**, 034029 (2017).
[21] M. D. Shaw, R. M. Lutchyn, P. Delsing, and P. M. Echternach, Phys. Rev. B **78**, 024503 (2008).
[22] S. M. Albrecht, E. B. Hansen, A. P. Higginbotham, F. Kuemmeth, T. S. Jespersen, J. Nygård, P. Krogstrup, J. Danon, K. Flensberg, and C. M. Marcus, Phys. Rev. Lett. **118**, 137701 (2017).
[23] F. W. J. Hekking, L. I. Glazman, K. A. Matveev, and R. I. Shekhter, Phys. Rev. Lett. **70**, 4138 (1993).
[24] M. Hell, K. Flensberg, and M. Leijnse, Phys. Rev. B **96**, 035444 (2017).
[25] D. V. Bulaev and D. Loss, Phys. Rev. B **71**, 205324 (2005).
[26] S. Takahashi, R. S. Deacon, K. Yoshida, A. Oiwa, K. Shibata, K. Hirakawa, Y. Tokura, and S. Tarucha, Phys. Rev. Lett. **104**, 246801 (2010).
[27] F. Nichele, S. Chesi, S. Hennel, A. Wittmann, C. Gerl, W. Wegscheider, D. Loss, T. Ihn, and K. Ensslin, Phys. Rev. Lett. **113**, 046801 (2014).
[28] A. P. Higginbotham, S. M. Albrecht, G. Kiršanskas, W. Chang, F. Kuemmeth, P. Krogstrup, T. S. Jespersen, J. Nygård, K. Flensberg, and C. M. Marcus, Nat. Phys. **11**, 1017 (2015).
[29] S. Vaitiekėnas, M.-T. Deng, J. Nygård, P. Krogstrup, and C. M. Marcus, Phys. Rev. Lett. **121**, 037703 (2018).
[30] C.-X. Liu, J. D. Sau, T. D. Stanescu, and S. Das Sarma, Phys. Rev. B **96**, 075161 (2017).
[31] S. Sasaki, S. Amaha, N. Asakawa, M. Eto, and S. Tarucha, Phys. Rev. Lett. **93**, 017205 (2004).